Identification of neural oscillations and epileptiform changes in human brain organoids

Ranmal A. Samarasinghe[1,2,3,4], Osvaldo A. Miranda[1,3,4], Simon Mitchell[5], Isabella Ferando[2], Momoko Watanabe[1,3,4], Jessie E. Buth[1,3,4], Arinnae Kurdian[1,3,4,6], Peyman Golshani[2,4,7,8] Kathrin Plath[3,9], William E. Lowry[3,10], Jack M. Parent[11,12], Istvan Mody[2,13], and Bennett G. Novitch[1,3,4,*]

[1]Department of Neurobiology, David Geffen School of Medicine at UCLA, Los Angeles, California, USA. [2]Department of Neurology, David Geffen School of Medicine at UCLA, Los Angeles, CA, USA. [3]Eli and Edythe Broad Center for Regenerative Medicine and Stem Cell Research, University of California, Los Angeles, Los Angeles, California, USA. [4]Intellectual Development and Disabilities Research Center, David Geffen School of Medicine at UCLA, Los Angeles, California USA. [5]Institute for Quantitative and Computational Biosciences, Department of Microbiology, Immunology, and Molecular Genetics, University of California, Los Angeles, California, USA. [6]California State University, Northridge, Northridge, California USA. [7]Semel Institute for Neuroscience and Human Behavior, University of California, Los Angeles, Los Angeles, California, USA. [8]West Los Angeles VA Medical Center, Los Angeles, California, USA. [9]Department of Biological Chemistry, David Geffen School of Medicine at UCLA, Los Angeles, CA, USA. [10]Department of Molecular, Cell, and Developmental Biology, University of California, Los Angeles, Los Angeles, California, USA. [11]Department of Neurology, University of Michigan Medical School, Ann Arbor, MI, USA. [12]Ann Arbor VA Healthcare System, University of Michigan Medical School, Ann Arbor, MI, USA. [13]Department of Physiology, David Geffen School of Medicine at UCLA, Los Angeles, California, USA.

*Corresponding author. Email: bnovitch@ucla.edu (B.G.N.)

ABSTRACT

Human brain organoids represent a powerful tool for the study of human neurological diseases particularly those that impact brain growth and structure. However, many neurological diseases lack obvious anatomical abnormalities, yet significantly impact neural network functions, raising the question of whether organoids possess sufficient neural network architecture and complexity to model these conditions. Here, we explore the network level functions of brain organoids using calcium sensor imaging and extracellular recording approaches that together reveal the existence of complex oscillatory network behaviors reminiscent of intact brain preparations. We further demonstrate strikingly abnormal epileptiform network activity in organoids derived from a Rett Syndrome patient despite only modest anatomical differences from isogenically matched controls, and rescue with an unconventional neuromodulatory drug Pifithrin-α. Together, these findings provide an essential foundation for the utilization of human brain organoids to study intact and disordered human brain network formation and illustrate their utility in therapeutic discovery.

INTRODUCTION

Brain organoids derived from human pluripotent stem cells have been shown to recapitulate unique features of human brain development and are increasingly being used as model systems to gain novel insights into a variety of neurological diseases[1-3]. Organoids represent a significant development in the toolkit available for of our understanding of brain function and disease mechanisms as much of our current knowledge is derived from studies of embryonic and adult animals, particularly rodents. While there is a great deal of conservation in the overall mechanisms of brain development across evolution, it has become increasingly clear that the human brain possesses many distinct features that are not shared with other species[4, 5], and it remains unclear how well animal models of neurological disease faithfully recapitulate human pathologies. Moreover, neuromodulatory drugs shown to be effective in ameliorating neurological disease in animals frequently fail when brought to clinical trials[6, 7], emphasizing the need for human cell-based systems to help evaluate drug efficacy.

Most brain organoid studies to date have capitalized on the anatomical and cytoarchitectural characteristics of the organoid to model disorders that grossly impact the growth or organization of the human brain such as microcephaly, macrocephaly, and lissencephaly[1-3]. However, the diverse functions of the human brain depend not only on its stereotyped anatomical structure, but also on the establishment and function of neural microcircuits, and their assembly into neural networks. Indeed, errors in the initial formation of these circuits or damage after their appropriate development are thought to underlie a number of neurological diseases ranging from autism spectrum and neuropsychiatric disorders to epilepsy and Alzheimer's disease[8, 9]. Reliably assessing network activity becomes especially critical in those situations in which there is clear clinical disease but no overt structural brain abnormality.

Despite ample evidence of the structural complexity of brain organoids, the presence of sophisticated neural network activities has not been comprehensively demonstrated in live whole-organoid preparations. A key identifying feature of robust neural networks is the presence of distinct frequencies of oscillatory activity. Such activities are thought to depend on precisely tuned inhibitory-excitatory neuronal interactions and can be recorded from intact brain preparations, but are not readily achievable in two-dimensional culture systems[10, 11]. In addition, specific changes in oscillatory activity, such as the loss of gamma activity or the emergence of polymorphic low frequency activity, can be clear indicators of underlying neurological dysfunction[12-14].

In the following study we sought to develop and characterize brain organoid network activity utilizing recent advances in organoid techniques[15] to generate cerebral cortex-ganglionic eminence (Cx+GE) "fusion" organoids in which excitatory and inhibitory neurons functionally integrate[16-18]. We then used a combination of calcium sensor imaging and extracellular recordings of local field potentials to demonstrate the presence of sophisticated network-level activities including oscillatory rhythms. These techniques allowed us to clearly discern pathological network and oscillatory changes in fusion organoids containing a mutation in the *Methyl-CpG Binding Protein 2* (*MECP2)* gene associated with Rett syndrome[19]. Collectively, these findings provide a framework for how brain organoids can be utilized to investigate the network-level functions of the human brain and illustrate their utility in modeling neurological disorders.

RESULTS

Fusion of cortex and ganglionic eminence organoids permits the assembly of abundant excitatory and inhibitory synaptic connections

As cortical circuits in vivo contain a mixture of both excitatory and inhibitory connections, we sought to replicate this process using an organoid "fusion" technique to combine separately generated cortical and subcortical organoids and create an integrated structure (Fig. 1 and Extended Data Fig. 1). Organoids were directed towards cortex (Cx) or ganglionic eminence (GE) identities through the absence or presence of Sonic hedgehog (Shh) pathway agonists in the organoid differentiation scheme (Fig. 1a)[15]. In the absence of Shh signaling, organoids predominantly exhibited cortical character including expression of the apical and basal radial glial progenitor marker PAX6, the intermediate progenitor marker TBR2 (EOMES), deep cortical plate markers including TBR1, CTIP2 (BCL11B), and BHLHB5 (BHLHE22), and superficial layer markers such as SATB2, and BRN2 (POU3F2) (Fig. 1b and Fig. 3a). Shh pathway-stimulated organoids by contrast expressed canonical GE progenitor and migratory interneuron markers such as NKX2.1, DLX1, DLX2, and OLIG2. Over time in culture, many neurons within the GE organoids expressed the general GABAergic inhibitory neuron marker GAD65 along with a variety of interneuron subtype markers including somatostatin (SST), calretinin, and calbindin (Fig. 1b and Extended Data Fig. 1c; see also[15]).

In the developing forebrain in vivo, GE-derived interneurons migrate tangentially into the adjacent cortex and functionally integrate into cortical neural networks, a process that can be recapitulated in vitro[16-18]. Using adeno-associated virus (AAV)-TdTomato labeling of the GE organoid before Cx+GE fusion, we observed widespread migration of TdTomato$^+$ cells originating from the GE and dispersion within the adjacent Cx two weeks after fusion (Fig. 1a,

c). Minimal TdTomato^{+} cell migration was seen in control Cx+Cx or Cx+GE fusions where Cx was pre-labeled with AAV-TdTomato (Fig. 1c). Immunohistochemical analyses of the cortical aspect of Cx+GE fusions revealed intermingling of Cx-derived excitatory neurons, exemplified by SATB2 which is not expressed within GE organoids, and inhibitory interneurons identified by GAD65 and DLX5 costaining (Fig. 1d). By contrast, Cx+Cx fusions only expressed the neuronal marker SATB2 with few if any GAD65^{+} DLX5^{+} cells (Fig. 1d). The integration of excitatory and inhibitory interneurons within the Cx+GE organoids was further confirmed by the prominence of both excitatory synapses, distinguished by VGLUT1 and PSD95 colocalization, and inhibitory synapses visualized by VGAT and gephyrin costaining (Fig. 1e). Cx+Cx organoids, in comparison, predominantly contained only excitatory synapses (Fig. 1e) showing that most inhibitory synapses in the Cx+GE organoids are GE-derived.

Cortex-ganglionic eminence fusion organoids exhibit complex neural network activities including interneuron-dependent multi-frequency oscillations

To determine the range of physiological activity in the fusion organoids, we utilized both live two-photon based calcium imaging of intact organoids and extracellular recordings of local field potentials (LFPs) (Fig. 2a). We applied constrained non-negative matrix factorization extended (CNMF-E) methods for calcium signal processing to extract spiking dynamics from records[20, 21], which enabled us to perform unbiased categorization of single cell calcium dynamics into functional microcircuit clusters (Extended Data Figs. 2, 3 and Supplementary Videos 1-3). In combination with LFP data, this approach allowed us to characterize brain organoid physiological activity at single cell, microcircuit, and network levels. After infection with AAV-GCaMP6f virus, we measured spontaneous calcium activity as changes in GCaMP6f

fluorescence (ΔF/F, Fig. 2b). Both Cx+Cx and Cx+GE fusions showed comparable spontaneous neural activities (Fig. 2c and Extended Data Fig. 3). However, when we assessed the role of inhibition by adding either the $GABA_A$ receptor antagonist bicuculline methiodide (BMI) or Gabazine, only Cx+GE fusions showed functional GABAergic interneuron-glutamatergic cell connectivity. Both drugs elicited repetitive waves of nearly complete synchronization of calcium transients in Cx+GE fusions (Fig. 2c, d), with no such effect in Cx+Cx fusions (Fig. 2c-e and Supplementary Videos 4-7). Hierarchical clustering revealed large groups of neurons with highly correlated activity in Cx+GE organoids following BMI treatment, while only small groups were observed in the Cx+Cx organoids (Fig. 2d).

LFP measurements in untreated fusion organoids uncovered simultaneous, sustained oscillations at multiple frequencies from 1-100 Hz in Cx+GE fusions (Fig. 2f-h), a hallmark of mature neural networks in vivo[22], while no discernible oscillatory activities were seen in Cx+Cx structures (Fig. 2, i to k). These findings suggest that the presence of GE-derived inhibitory interneurons stimulates maturation of excitatory cortical networks, as has been shown in the rodent brain[23, 24]. Moreover, these data indicate that interneurons uniquely entrain the behavior of excitatory cells in Cx+GE fusions, and that the resultant networks are capable of producing complex oscillations resembling those observed by extra- and intracranial recordings of the intact human brain.

Rett syndrome fusion organoids exhibit hypersynchronous neural network activities

We next used this platform to measure pathophysiological changes associated with human neurological disease. Rett syndrome is a neurodevelopmental disorder typically caused by de novo mutations in one copy of the *MECP*2 gene on the X chromosome, where affected females

exhibit symptoms as early as seven months of age[25]. Rett female patients exhibit motor delays, cognitive and neuropsychiatric disturbances, autism, and epilepsy[25]. However, these changes likely present well before clinical symptoms. For example, a recent hiPSC-based study has suggested that Rett may impact prenatal neurogenesis through microRNA-mediated changes in AKT and ERK activity[26]. Interestingly, while neuroanatomical changes in dendritic arborization and spine density have been reported in multiple Rett models[25, 27-30], gross structural abnormalities are less prevalent.

Due to random X-chromosome inactivation, Rett patients are typically mosaic in their *MECP2* status, with some cells expressing and others lacking a functional *MECP2* allele. This feature permitted the generation of isogenic hiPSC from a single patient as hiPSC reprograming does not revert X-chromosome silencing[30]. We accordingly generated Cx and GE organoids from isogenic control (iCtrl) and *MECP2*-mutant (Mut) Rett syndrome patient hiPSC and found no obvious differences in their cytoarchitecture or cell composition (Fig. 3, a and b). The cortex region of both iCtrl and Mut Cx+GE fusions also contained similar percentages of GAD65^{+} interneurons (mean ~25%; Fig. 3, c and d), comparable to the percentages reported in most mammalian species[31]. VGLUT1/PSD95 costaining showed that the abundance of excitatory synapses was nevertheless slightly increased in Mut fusion organoids relative to iCtrl, while VGAT/gephyrin^{+} inhibitory synapses were not significantly different (Fig. 3, e and f), suggesting that the Mut fusion organoids may be prone to hyperexcitability.

More striking, however, were activity differences revealed though GCaMP6f imaging. Mut Cx+GE fusions exhibited epochs of spontaneously synchronized calcium transients (Fig. 3, g and h, and Supplementary Videos 8-9) reminiscent of the synchronizations observed following administration of $GABA_A$ receptor antagonists to control samples (Fig. 2, c to e and

Supplementary Videos 4-5) and the epileptiform changes seen in murine models of Rett syndrome[32]. Previous reports have indicated increased overall activity and diminished size of neural microcircuits in mouse chemoconvulsant epilepsy models[33]. We similarly observed that the increased synchronization of calcium transients in Mut Cx+GE organoids was accompanied by reductions in both the size of microcircuit clusters and the number of neurons within each cluster (Extended Data Fig. 4a).

Rett syndrome fusion organoids display deficits in low-frequency oscillations and frequent appearance of epileptiform high-frequency oscillations

LFP recordings of iCtrl Cx+GE fusions demonstrated infrequent spikes and sustained low frequency and gamma oscillations with few epochs of higher frequency oscillations (> 100 Hz) as was observed with H9 hESC-derived fusion organoids (Fig. 4, a to e, compare to Fig. 2d). By contrast, Mut Cx+GE organoids lacked low frequency and gamma oscillations (Fig. 4, b and c) and instead exhibited recurring epileptiform-appearing spikes and high frequency oscillations (HFOs, ~200-500 Hz; Fig. 4, a, d, e and Extended Data Fig. 5). These findings concurred with calcium imaging data which showed rare but large high amplitude calcium synchronizations in Mut fusion organoids that could result in spikes or HFOs, as opposed to the numerous small synchronizations seen in iCtrl samples which likely generate sustained lower frequency oscillations without epileptiform events (Fig. 3i and Extended Data Fig. 4b). Hypersynchrony, HFOs, and spikes seen in Mut Cx-GE organoids are all consistent with the electrographic changes observed in human epilepsy[34, 35]. Indeed, electroencephalographic abnormalities were documented in the Rett patient whose hiPSCs were used in this study[30].

Epilepsy is present in 60-80% of Rett patients and is thought to arise primarily from interneuron dysfunction[36, 37], though *MECP2* loss in other cell types has been implicated in the syndrome[19]. As our Cx and GE organoids are respectively enriched in excitatory vs. inhibitory interneurons, we generated "mixed" fusions in which either the Cx or GE half of the fused structure was Mut while the other half was iCtrl, as a means of determining the compartment and cell type in which *MECP2* deficiency matters most. Mut Cx+iCtrl GE mixed-fusion organoids displayed an LFP profile nearly identical to unmixed iCtrl Cx+GE fusions (Fig. 4, a to e and Extended Data Fig. 5). By contrast, iCtrl Cx+Mut GE organoids demonstrated frequent spikes and HFOs along with deficits in distinct lower frequency activity, similar to unmixed Mut Cx+GE fusions (Fig. 4, a to e and Extended Data Fig. 5), suggesting that *MECP2* deficiency in GE-derived interneurons drives the observed changes in network function. Consistent with this conclusion, overall spike frequency was significantly increased in unmixed Mut Cx+GE organoids and iCtrl Cx+Mut GE mixed-fusions compared to iCtrl Cx+GE or Mut Cx+iCtrl GE structures (Fig. 4f).

Both human and murine in vivo studies have shown an inverse relationship between gamma band power and epileptiform discharges[12, 13]. Gamma oscillations are thought to require complex inhibitory-excitatory network interactions that are highly prone to disruption by epileptic or interictal discharges[12]. In agreement with this, we routinely observed gamma oscillations in unmixed iCtrl Cx+GE and mixed Mut Cx+iCtrl GE organoids and rarely recorded spiking activity in these samples. In contrast, we observed significant reductions of gamma oscillations in Mut Cx+GE and iCtrl Cx+Mut GE structures (Fig. 4g) coincident with frequent epileptiform spikes and HFOs (Fig. 4d).

Neural oscillation defects seen in Rett syndrome fusion organoids can be partially restored by administration of an unconventional neuromodulatory drug Pifithrin-α

A heralded, but largely unrealized, application of patient-derived hiPSCs is in personalized medicine. We therefore sought to determine the utility of the epileptiform phenotype observed in Rett syndrome organoids for drug testing. First, we used a broad-spectrum anti-seizure medication, sodium valproate (VPA), which is commonly used to treat epilepsy resulting from Rett Syndrome[38]. We also tested the effect of a putative TP53 target inhibitor, Pifithrin-α, based on previous studies showing that *MECP2* deficiency leads to over-activation of the TP53 pathway and premature neuronal senescence[30, 39]. Consistent with its known spike suppressant properties, exposure to VPA significantly reduced spiking activity in the Mut Cx+GE organoids (Fig. 5, a and c), although it neither decreased HFOs nor restored lower frequency oscillations (Fig. 5, b and d). Pifithrin-α similarly reduced spike frequency but remarkably also suppressed HFOs and resulted in the re-emergence of gamma oscillations (Fig. 5, a to d). These results suggest that unlike VPA, which appeared to merely reduce neuronal hyperexcitability, Pifithrin-α may modulate more upstream excitatory-inhibitory physiologic interactions resulting in a more global restoration of network-level functions. These findings further illustrate the potential value of the fusion organoid modeling approach in personalized drug discovery.

DISCUSSION

Collectively, these experiments demonstrate the existence of highly sophisticated physiological activities within Cx+GE organoids, congruent with their cytoarchitectural and cellular complexity. These results stand in agreement with findings recently reported by Trujillo et al,

who have also observed the emergence of neural oscillations in cortical organoids cultured for prolonged time periods using a different recording approach[40]. Our studies here further demonstrate that the emergence of higher order network activities such as multi-frequency oscillations requires functional integration of inhibitory interneurons into the excitatory network framework as permitted by the organoid fusion technique, since no oscillations were apparent without them. Critically, this approach also allowed us to identify striking electrophysiological phenotypes in *MECP2* mutant Cx+GE organoids despite their cytoarchitectural similarity to iCtrl samples. Nevertheless, we observed a modest increase in excitatory but not inhibitory synaptic puncta in Mut organoids consistent with their overall level of hyperactivity and hypersynchrony. The fusion organoid approach also enabled us to demonstrate that *MECP2* mutation restricted to GE derivatives, most notably inhibitory interneurons, was sufficient to drive epileptiform-like LFP changes, suggesting that multifactorial excitatory-inhibitory cell interactions underlie the *MECP2*-deficient phenotype. Interestingly, we achieved a more complete rescue of the Mut phenotype with a novel drug, Pifithrin-α, than was seen with a traditional anti-seizure medication, VPA, meriting future investigations into its neuromodulatory actions.

In summary, these findings illustrate the potential of brain organoids both as a unique platform for characterizing human neural networks and for personalized drug discovery and research. A remaining challenge is to delineate the precise microcircuit and cell type-specific perturbations that underlie both the oscillatory and pathological epileptiform-like changes revealed in these studies. The fusion organoid system is highly amenable to such detailed cellular and circuit analyses and provides unprecedented opportunities for modeling neural network dysfunction associated with a variety of human neurological disorders.

REFERENCES

1. Di Lullo, E. & Kriegstein, A.R. The use of brain organoids to investigate neural development and disease. *Nat Rev Neurosci* **18**, 573-584 (2017).
2. Amin, N.D. & Pasca, S.P. Building Models of Brain Disorders with Three-Dimensional Organoids. *Neuron* **100**, 389-405 (2018).
3. Qian, X., Song, H. & Ming, G.L. Brain organoids: advances, applications and challenges. *Development* **146** (2019).
4. Rakic, P. Evolution of the neocortex: a perspective from developmental biology. *Nat Rev Neurosci* **10**, 724-735 (2009).
5. Molnar, Z., et al. Evolution and development of the mammalian cerebral cortex. *Brain Behav Evol* **83**, 126-139 (2014).
6. van der Worp, H.B., et al. Can animal models of disease reliably inform human studies? *PLoS Med* **7**, e1000245 (2010).
7. Dawson, T.M., Golde, T.E. & Lagier-Tourenne, C. Animal models of neurodegenerative diseases. *Nat Neurosci* **21**, 1370-1379 (2018).
8. Stam, C.J. Modern network science of neurological disorders. *Nat Rev Neurosci* **15**, 683-695 (2014).
9. Palop, J.J. & Mucke, L. Network abnormalities and interneuron dysfunction in Alzheimer disease. *Nat Rev Neurosci* **17**, 777-792 (2016).
10. Buzsaki, G. & Wang, X.J. Mechanisms of gamma oscillations. *Annu Rev Neurosci* **35**, 203-225 (2012).
11. Headley, D.B. & Pare, D. Common oscillatory mechanisms across multiple memory systems. *NPJ Sci Learn* **2** (2017).

12. Verret, L., et al. Inhibitory interneuron deficit links altered network activity and cognitive dysfunction in Alzheimer model. *Cell* **149**, 708-721 (2012).

13. Matsumoto, J.Y., et al. Network oscillations modulate interictal epileptiform spike rate during human memory. *Brain* **136**, 2444-2456 (2013).

14. van Dellen, E., et al. Local polymorphic delta activity in cortical lesions causes global decreases in functional connectivity. *Neuroimage* **83**, 524-532 (2013).

15. Watanabe, M., et al. Self-Organized Cerebral Organoids with Human-Specific Features Predict Effective Drugs to Combat Zika Virus Infection. *Cell Rep* **21**, 517-532 (2017).

16. Bagley, J.A., Reumann, D., Bian, S., Levi-Strauss, J. & Knoblich, J.A. Fused cerebral organoids model interactions between brain regions. *Nat Methods* **14**, 743-751 (2017).

17. Birey, F., et al. Assembly of functionally integrated human forebrain spheroids. *Nature* **545**, 54-59 (2017).

18. Xiang, Y., et al. Fusion of Regionally Specified hPSC-Derived Organoids Models Human Brain Development and Interneuron Migration. *Cell Stem Cell* **21**, 383-398 e387 (2017).

19. Lyst, M.J. & Bird, A. Rett syndrome: a complex disorder with simple roots. *Nat Rev Genet* **16**, 261-275 (2015).

20. Pnevmatikakis, E.A., et al. Simultaneous Denoising, Deconvolution, and Demixing of Calcium Imaging Data. *Neuron* **89**, 285-299 (2016).

21. Zhou, P., et al. Efficient and accurate extraction of in vivo calcium signals from microendoscopic video data. *Elife* **7** (2018).

22. Buzsaki, G. & Draguhn, A. Neuronal oscillations in cortical networks. *Science* **304**, 1926-1929 (2004).

23. Wang, D.D. & Kriegstein, A.R. GABA regulates excitatory synapse formation in the neocortex via NMDA receptor activation. *J Neurosci* **28**, 5547-5558 (2008).

24. Wang, D.D. & Kriegstein, A.R. Blocking early GABA depolarization with bumetanide results in permanent alterations in cortical circuits and sensorimotor gating deficits. *Cereb Cortex* **21**, 574-587 (2011).

25. Leonard, H., Cobb, S. & Downs, J. Clinical and biological progress over 50 years in Rett syndrome. *Nat Rev Neurol* **13**, 37-51 (2017).

26. Mellios, N., et al. MeCP2-regulated miRNAs control early human neurogenesis through differential effects on ERK and AKT signaling. *Mol Psychiatry* **23**, 1051-1065 (2018).

27. Armstrong, D.D., Dunn, K. & Antalffy, B. Decreased dendritic branching in frontal, motor and limbic cortex in Rett syndrome compared with trisomy 21. *J Neuropathol Exp Neurol* **57**, 1013-1017 (1998).

28. Belichenko, P.V., et al. Widespread changes in dendritic and axonal morphology in Mecp2-mutant mouse models of Rett syndrome: evidence for disruption of neuronal networks. *J Comp Neurol* **514**, 240-258 (2009).

29. Marchetto, M.C., et al. A model for neural development and treatment of Rett syndrome using human induced pluripotent stem cells. *Cell* **143**, 527-539 (2010).

30. Ohashi, M., et al. Loss of MECP2 Leads to Activation of P53 and Neuronal Senescence. *Stem Cell Rep* **10**, 1453-1463 (2018).

31. Sahara, S., Yanagawa, Y., O'Leary, D.D. & Stevens, C.F. The fraction of cortical GABAergic neurons is constant from near the start of cortical neurogenesis to adulthood. *J Neurosci* **32**, 4755-4761 (2012).

32. Lu, H., et al. Loss and Gain of MeCP2 Cause Similar Hippocampal Circuit Dysfunction that Is Rescued by Deep Brain Stimulation in a Rett Syndrome Mouse Model. *Neuron* **91**, 739-747 (2016).

33. Feldt Muldoon, S., Soltesz, I. & Cossart, R. Spatially clustered neuronal assemblies comprise the microstructure of synchrony in chronically epileptic networks. *Proc Natl Acad Sci U S A* **110**, 3567-3572 (2013).

34. Bragin, A., Engel, J., Jr., Wilson, C.L., Fried, I. & Buzsaki, G. High-frequency oscillations in human brain. *Hippocampus* **9**, 137-142 (1999).

35. Bragin, A., Wilson, C.L., Almajano, J., Mody, I. & Engel, J., Jr. High-frequency oscillations after status epilepticus: epileptogenesis and seizure genesis. *Epilepsia* **45**, 1017-1023 (2004).

36. Ito-Ishida, A., Ure, K., Chen, H., Swann, J.W. & Zoghbi, H.Y. Loss of MeCP2 in Parvalbumin-and Somatostatin-Expressing Neurons in Mice Leads to Distinct Rett Syndrome-like Phenotypes. *Neuron* **88**, 651-658 (2015).

37. Krajnc, N. Management of epilepsy in patients with Rett syndrome: perspectives and considerations. *Ther Clin Risk Manag* **11**, 925-932 (2015).

38. Vignoli, A., et al. Effectiveness and tolerability of antiepileptic drugs in 104 girls with Rett syndrome. *Epilepsy Behav* **66**, 27-33 (2017).

39. Squillaro, T., et al. Reduced expression of MECP2 affects cell commitment and maintenance in neurons by triggering senescence: new perspective for Rett syndrome. *Mol Biol Cell* **23**, 1435-1445 (2012).

40. Trujillo, C.A., et al. Complex Oscillatory Waves Emerging from Cortical Organoids Model Early Human Brain Network Development. *Cell Stem Cell*, 10.1016/j.stem.2019.1008.1002 (2019).

METHODS

hESC and hiPSC culture and organoid generation. All hPSC experiments were conducted following prior approval from the University of California Los Angeles (UCLA) Embryonic Stem Cell Research Oversight Committee (ESCRO) and Institutional Review Board. Cortex (Cx) and ganglionic eminence (GE) organoids were generated from the H9 hPSC line[41] or Rett hiPSCs[30] as described previously[15] and outlined in schematic form in Fig 1a. Fusion was performed with minor modifications as previously reported[17]. Cx and GE Organoids were cut at day 56 and two halves (e.g. Cx+GE or Cx+Cx) were combined in a microcentrifuge tube containing 300µl of N2B27 media[15] and placed in a hyperoxic incubator containing 5% CO_2 and 40% O_2 for 72 hours. Fused structures were then carefully transferred to 24-well oxygen permeable dishes (Lumox, Sarstedt) and maintained in a hyperoxic environment with media changes every other day until their use. Neuron migration experiments were conducted by infection of either a Cx or GE organoid with 5 µl of ~1.98×10^{13} ml^{-1} AAV1-TdTomato (pENN.AAV.CAG.tdTomato.WPRE.SV40, a gift of Dr. James M. Wilson, University of Pennsylvania Vector Core AV-1-PV3365) on day 56 and fusion was performed as described 3 days after infection.

Generation of Rett hiPSCs. Rett iPSCs were derived from fibroblast line GM07982 obtained from Coriell Repositories and generated by lentiviral transduction of the cells with the Yamanaka factors (Oct4, Klf4, Sox2, and cMyc) as previously described[30]. GM07982 cells were isolated from a 25-year-old female noted to have EEG abnormalities, and found to contain a truncating frameshift mutation, 705delG, in the *MECP2* gene. As Rett females are typically heterozygous for the *MECP2* mutation, the collected fibroblasts are mosaic in their MECP2

status with approximately half of the cells expressing the non-mutant allele. Unlike murine cells, the inactive X chromosome remains inactive after reprograming to pluripotency[42], allowing the generation *MECP2* mutant (Mut) and isogenic control (iCtrl) hiPSCs from the same patient fibroblasts.

Immunohistochemistry. Organoids were immersion fixed in 4% paraformaldehyde, cryoprotected in 30% sucrose, frozen in Tissue-Tek Optimal Cutting Temperature (O.C.T., Sakura) media, and cryosectioned. Immunostaining was performed using previously published laboratory protocols[15, 43]. Primary antibodies used include the following: goat anti-BRN2 (POU3F2; Santa Cruz Biotechnology sc-6029), 1:4000; mouse anti-CALBINDIN (Clone CB-955, Sigma-Aldrich C9848), 1:5000; rabbit anti-CALRETININ (EMD Millipore AB5054), 1:2000; rat anti-CTIP2 (BCL11B; Abcam ab18465), 1:1000; rabbit anti-DLX1[44] (generous gift of Drs. Soo Kyung Lee and Jae Lee), 1:3000; guinea pig anti-DLX2[45] (generous gift of Drs. Kazuaki Yoshikawa and Hideo Shinagawa), 1:3000; guinea pig anti-DLX5[45] (generous gift of Drs. Kazuaki Yoshikawa and Hideo Shinagawa), 1:3000; rabbit anti-FOXG1 (Abcam ab18259), 1:1000; rabbit anti-GABA (Sigma-Aldrich A2052), 1:10000; mouse anti-GAD65 (BD Biosciences 559931), 1:200; mouse anti-GEPHYRIN (Synaptic Systems 147021), 1:500; goat anti-LHX2 (C-20, Santa Cruz Biotechnology sc-19344), 1:1000; rabbit anti-MECP2 (Diagenode C15410052), 1:1000; mouse anti-N-CADHERIN (CDH2, BD Biosciences 610920), 1:1000; mouse anti-NKX2.1 (Novocastra NCL-L-TTR-1), 1:500; mouse anti-PAX6 (Developmental Studies Hybridoma Bank), 1:100; rabbit anti-PAX6 (MBL International PD022), 1:1000; mouse anti-PSD95 (Millipore MAB1598), 1:1000; mouse anti-SATB2 (Abcam ab51502), 1:100; goat anti-SOX2 (Santa Cruz Biotechnology sc-17320, 1:100; rat ant-SOMATOSTATIN (SST, EMD

Millipore MAB354), 1:100; rabbit anti-TBR1 (Abcam ab31940), 1:2000; chicken anti-TBR2 (EOMES; EMD Millipore AB15894), 1:1000; guinea pig anti-VGAT (Synaptic Systems 131004), 1:1000; guinea pig anti-VGLUT1 (SLC17A7; EMD Millipore AB5905), 1:1000. Secondary antibody staining was conducted using Dylight 405-, FITC-, Alexa 488-, Cy3-, Alexa 594-, Cy5-, Alexa 647, Dylight 647-conjugated donkey anti-species-specific IgG or IgM antibodies (Jackson ImmunoResearch or Invitrogen/Molecular Probes). Nuclei were often counterstained using Hoechst 33258 added to the secondary antibody mix at a final concentration of 1 $\mu g\ ml^{-1}$. Images were primarily obtained on a Zeiss LSM 800 confocal microscope except for synaptic puncta, which were imaged using a 63X objective on a Zeiss LSM 880 confocal microscope equipped with Airyscan technology. All images that were directly compared were obtained with identical laser power settings. Image adjustments were limited to brightness, contrast, and level and were applied equally to all images in a set being compared.

Cell and synaptic puncta quantification. All cell quantifications were obtained using at least 9 images per sample consisting of 3 non-contiguous regions per image and at least 3 images obtained from independent experiments. For GAD65 quantification, tiled images of fusion or un-fused organoids were visualized in Photoshop (Adobe), a box of equal size was used to demarcate regions of interest on the outer edges of organoids, and total numbers of $GAD65^+$ cells and $Hoechst^+$ nuclei within the boxed region were manually tabulated. Synaptic puncta were identified and colocalized using Imaris image processing software (Bitplane) using the "spots" identifier, set to detect identically sized objects and thresholded against Hoechst staining to exclude any nuclear overlap. The native "colocalization" function on Imaris was used to identify overlapping puncta.

Live organoid calcium imaging. The genetically encoded calcium indicator GCaMP6f was introduced into organoids between day 88-95 via infection with 5 µl of 1.98×10^{13} GC ml^{-1} pAAV1.Syn.GCaMP6f.WPRE.SV40 virus[46], a gift from Dr. Douglas Kim & the GENIE Project (Addgene viral prep # 100837-AAV1 or UPENN Vector core AV-1-PV2822). All imaging was performed 12-14 days after infection using a Scientifica two-photon microscope with a Coherent Chameleon tunable laser. Calcium transients were recorded at an excitation of 920 nm using a 20X 0.8NA water-immersion objective (Nikon) and at a frame rate of 31 Hz with 512 x 512-pixel resolution and 0.5 x 0.5 mm field of view. Recording was performed in artificial cerebrospinal fluid (aCSF) as described below with additional 10mM HEPES to maintain a pH of 7.3-7.4 in the absence of O_2/CO_2 perfusion (see Extracellular Recording below for details). Following initial imaging in the absence of drugs, organoids were then subjected to 1-minute incubation with the $GABA_A$ receptor antagonist gabazine (25 µM) or bicuculline methiodide (100 µM) and the identical fields were re-imaged after drug exposure.

Microcircuit identification. Raw Ca^{2+} imaging files in tiff format were processed to identify fluorescence transients ($\Delta F/F_0$) and spike estimation in MATLAB (Mathworks Inc.) using the constrained non-negative matrix factorization-extended (CNMF-E) methodology[20, 21]. Following CNMF-E based data extraction neuronal microcircuit clusters were identified by performing hierarchical clustering on the correlation matrix of neuronal Ca^{2+} spiking data and analyzed based on Muldoon et al.[33]. The correlation between all pair-wise combinations of the time course of spikes for all neurons identified by CNMF-E was calculated to generate a correlation matrix. Following generation of the correlation matrix, linkage analysis was performed using the

MATLAB *linkage* function from the statistics toolbox (with 'complete'/furthest distance). The generated hierarchical clustering was input into the *dendrogram* function from the MATLAB statistics toolbox with *'Color Threshold'* fixed at 1.5 for all experimental groups. By then assigning each neuron to a cluster determined by its assigned color in the dendrogram, clusters were created in which there was high correlation between all neurons in the cluster. In order to calculate the number of pairs of neurons that were significantly correlated within each dataset we first generated 1000 shuffled time courses for each neuron using MATLAB's *randperm* function. Pairwise correlations for the randomly shuffled time courses were calculated in the same way as the original data, and a pair of neurons were considered correlated if their correlation coefficient in the original data was significantly different to the 1000 shuffled datasets with $P < 0.05$. To determine the threshold of simultaneous firing, the synchronization of the time shuffled data was calculated, and the threshold was set at the 99th percentile of synchronization in the shuffled data. Synchronization above this threshold was considered "synchronized". These data were then plotted on a normalized y-axis ranging from 0 (no synchronizations) to 1 (100% synchronization) and time on the x-axis. The total number of synchronizations, average synchronization amplitude, and average synchronization duration were then tabulated.

Extracellular recordings. Organoids were recorded between age day ~100-107. Live organoids were perfused with 500nM kainic acid in aCSF (containing in mM: NaCl 126, D-glucose 10, $MgCl_2$ 1.2, $CaCl_2$ 2, KCl 5, NaH_2PO_4 1.25, Na Pyruvate 1.5, L-Glutamine 1, $NaHCO_3$ 26, pH 7.3-7.4 when bubbled with 95% O_2, 5% CO_2) to initiate oscillatory network activity. LFP activity was recorded using a patch pipette filled with aCSF connected with a head stage to a field amplifier (A-M Systems Inc., model 3000), and band pass filtered between 0.1 and 1000 Hz

by to an instrumentation amplifier (Brownlee BP Precision, model 210A). Field potentials were digitized at 4096 Hz with a National Instruments A/D board using EVAN (custom-designed LabView-based software from Thotec) and analyzed with custom procedures (Wavemetrics, Igor Pro 8). Lower frequency activity was visualized for 10-minute epochs using power spectral densities (PSDs), which were calculated using the "dsperiodogram" function of Igor Pro, and spectrograms, which were generated using the Gabor method on Igor Pro. High frequency activity up to 650 Hz was visualized by generating Morlet wavelet plots of 0.5-1.0 second epochs of the raw traces used for low frequency analyses. Inter-spike intervals and spike frequencies were tabulated on Igor Pro using the identical 10-minute epochs used above.

Statistical information. All samples were subject to Shapiro-Wilk and Kolmogorov-Smirnov normality testing. Non-normal samples were analyzed by a two-tailed Mann-Whitney U-test or Kruskal-Wallis test followed by Dunn's multiple comparison test. Normally distributed data were analyzed by a two-tailed Student's *t*-test or ANOVA with post hoc Tukey's multiple comparison test. Violin plots display the full distribution of individual data points with dotted lines to indicate the median and quartile values. Figure legends specify sample numbers and *P* values for all statistical tests. Each *n* represents an independent experiment. Table S1 specifies the number of non-contiguous sections imaged prior to selection of representative images. The *n* for all other representative images is specified in the figure legends.

DATA AVAILABILITY

The authors declare that all data supporting the findings of this study are available within the paper and its supplementary information files.

CODE AVAILABILITY

CNMF/CNMF-E has been previously published. CNMF_E is publicly available on Github at https://github.com/zhoupc/CNMF_E *(6)*.

SUPPLEMENTARY REFERENCES

41. Thomson, J.A., et al. Embryonic stem cell lines derived from human blastocysts. *Science* **282**, 1145-1147 (1998).
42. Tchieu, J., et al. Female human iPSCs retain an inactive X chromosome. *Cell Stem Cell* **7**, 329-342 (2010).
43. Rousso, D.L., Gaber, Z.B., Wellik, D., Morrisey, E.E. & Novitch, B.G. Coordinated actions of the forkhead protein Foxp1 and Hox proteins in the columnar organization of spinal motor neurons. *Neuron* **59**, 226-240 (2008).
44. Lee, B., et al. Dlx1/2 and Otp coordinate the production of hypothalamic GHRH- and AgRP-neurons. *Nat Commun* **9**, 2026 (2018).
45. Kuwajima, T., Nishimura, I. & Yoshikawa, K. Necdin promotes GABAergic neuron differentiation in cooperation with Dlx homeodomain proteins. *J Neurosci* **26**, 5383-5392 (2006).
46. Chen, T.W., et al. Ultrasensitive fluorescent proteins for imaging neuronal activity. *Nature* **499**, 295-300 (2013).

ACKNOWLEDGEMENTS

We thank S. Butler, T. Carmichael, and members of the Novitch lab for helpful discussions and comments on the manuscript; J. Buth, N. Vishlaghi, and F. Turcios-Hernandez for technical assistance, and J. Lee, S.-K. Lee, H. Shinagawa, and K. Yoshikawa for valuable reagents. We also thank the UCLA Broad Stem Cell Research Center (BSCRC) and Intellectual and Developmental Disabilities Research Center microscopy cores for access to imaging facilities. This work was supported by research awards from the UCLA Jonsson Comprehensive Cancer Center, and BSCRC Ablon Scholars Program, the Dave Steffy Stem Cell Research Fund, the UCLA Clinical and Translational Science Institute, and grants from the California Institute for Regenerative Medicine (CIRM) (DISC1-08819 to B.G.N.), the National Institute of Health (R01NS089817 and R01NS085227 to B.G.N.; R01NS088571 to J.M.P.; R01NS030549 and R01AG050474 to I.M.), the Paul Allen Family Foundation Frontiers Group to K.P. and W.E.L., and the March of Dimes Foundation to W.E.L. R.A.S. was supported by the UCLA/NINDS Translational Neuroscience Training Grant (R25NS065723), a Research and Training Fellowship from the American Epilepsy Society, and a training award from the UCLA BSCRC. M.W. was supported by postdoctoral training awards provided by the UCLA BSCRC and the Uehara Memorial Foundation, and a grant from the NICHD (K99HD096105). O.A.M. and A.K. were supported in part by the UCLA-California State University Northridge CIRM-Bridges training program (EDUC2-08411). We also acknowledge the support of the IDDRC Cells, Circuits and Systems Analysis, Microscopy and Genetics and Genomics Cores of the Semel Institute of Neuroscience at UCLA, which are supported by the NICHD (U54HD087101).

AUTHOR CONTRIBUTIONS

R.A.S, O.A.M, A.K., and J.M.P. performed most of the organoid culture experiments and R.A.S. worked with others below on various analytical procedures. M.W., J.E.B., and B.G.N. assisted with the development of the organoid culture methods. B.G.N. assisted with imaging analysis. S.M. assisted R.A.S. in computational analysis of calcium indicator imaging experiments. I.F. and I.M. provided expertise in local field potential recording methods and data analysis. P.G. provided guidance in 2-photon calcium indicator imaging and computational methods. K.P and W.E.L. provided the Rett patient hiPSC used in the experiments. R.A.S., J.M.P., and B.G.N. conceived, designed, and supervised the experiments with helpful input from the other authors. R.A.S. and B.G.N. wrote the manuscript.

COMPETING INTERESTS

The authors declare no competing interests.

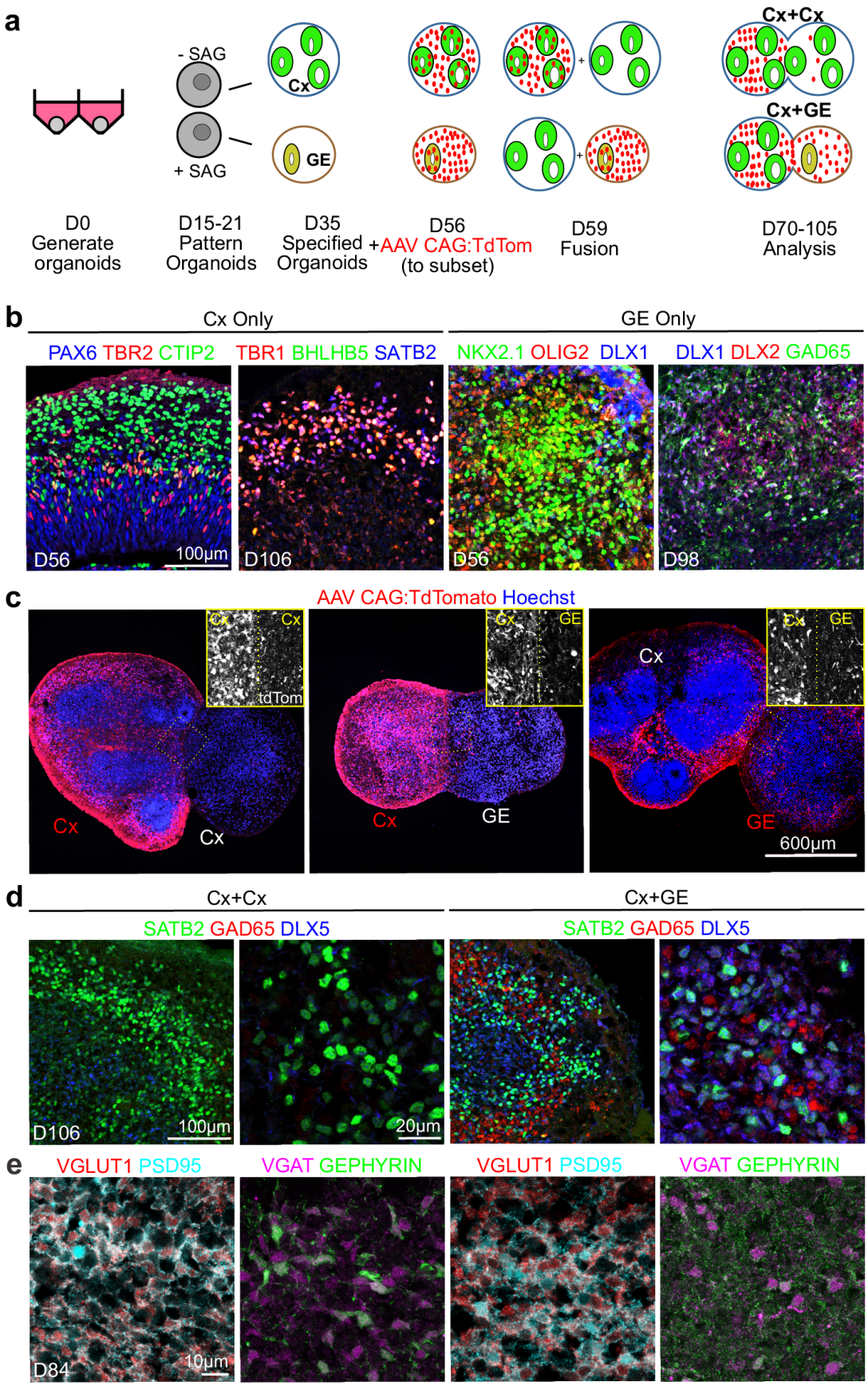
a
- SAG
+ SAG
Cx
GE
Cx+Cx
Cx+GE
D0
Generate
organoids
D15-21
Pattern
Organoids
D35
Specified
Organoids
D56
+AAV CAG:TdTom
(to subset)
D59
Fusion
D70-105
Analysis
b
Cx Only
GE Only
PAX6 TBR2 CTIP2
TBR1 BHLHB5 SATB2
NKX2.1 OLIG2 DLX1
DLX1 DLX2 GAD65
D56
100µm
D106
D56
D98
c
AAV CAG:TdTomato Hoechst
Cx
tdTom
GE
600µm
d
Cx+Cx
Cx+GE
SATB2 GAD65 DLX5
D106
100µm
20µm
e
VGLUT1 PSD95
VGAT GEPHYRIN
D84
10µm

Fig. 1 | Generation and characterization of fusion brain organoids. (**a**) Schematic outlining the generation, patterning, and fusion of dorsal cortex (Cx) and ventral ganglionic eminence (GE) organoids. (**b**) Immunohistochemical analysis of H9 hESC or non-mutant hiPSC-derived Cx and GE organoids prior to fusion at the indicated days (D) of differentiation in vitro. (**c**) Prior to fusion, D56 Cx or GE organoids were infected with AAV1-CAG:TdTomato virus, allowing for tracking of cells emanating from each compartment. Two weeks after fusion, labeled Cx cells showed limited migration into adjacent Cx or GE structures (left and middle images) while labeled GE progenitors display robust migration and colonization of their Cx partner (right image). (**d**) Immunohistochemical analysis showing intermingling of SATB2$^+$ cortical neurons with DLX5$^+$ GAD65$^+$ inhibitory interneurons in the cortical compartment of D106 Cx+GE but not Cx+Cx fusion organoids. (**e**) At day 84, Cx+Cx fusions (left panels) contain numerous excitatory synapses reflected by prominent colocalization of the pre- and post-synaptic markers VGLUT1 and PSD95, yet sparse numbers of inhibitory synapses detected by VGAT/GEPHYRIN costaining. Cx+GE fusions (right panels) on the other hand contain numerous VGLUT1$^+$/PSD95$^+$ excitatory and VGAT$^+$/GEPHYRIN$^+$ inhibitory synapses (right panels).

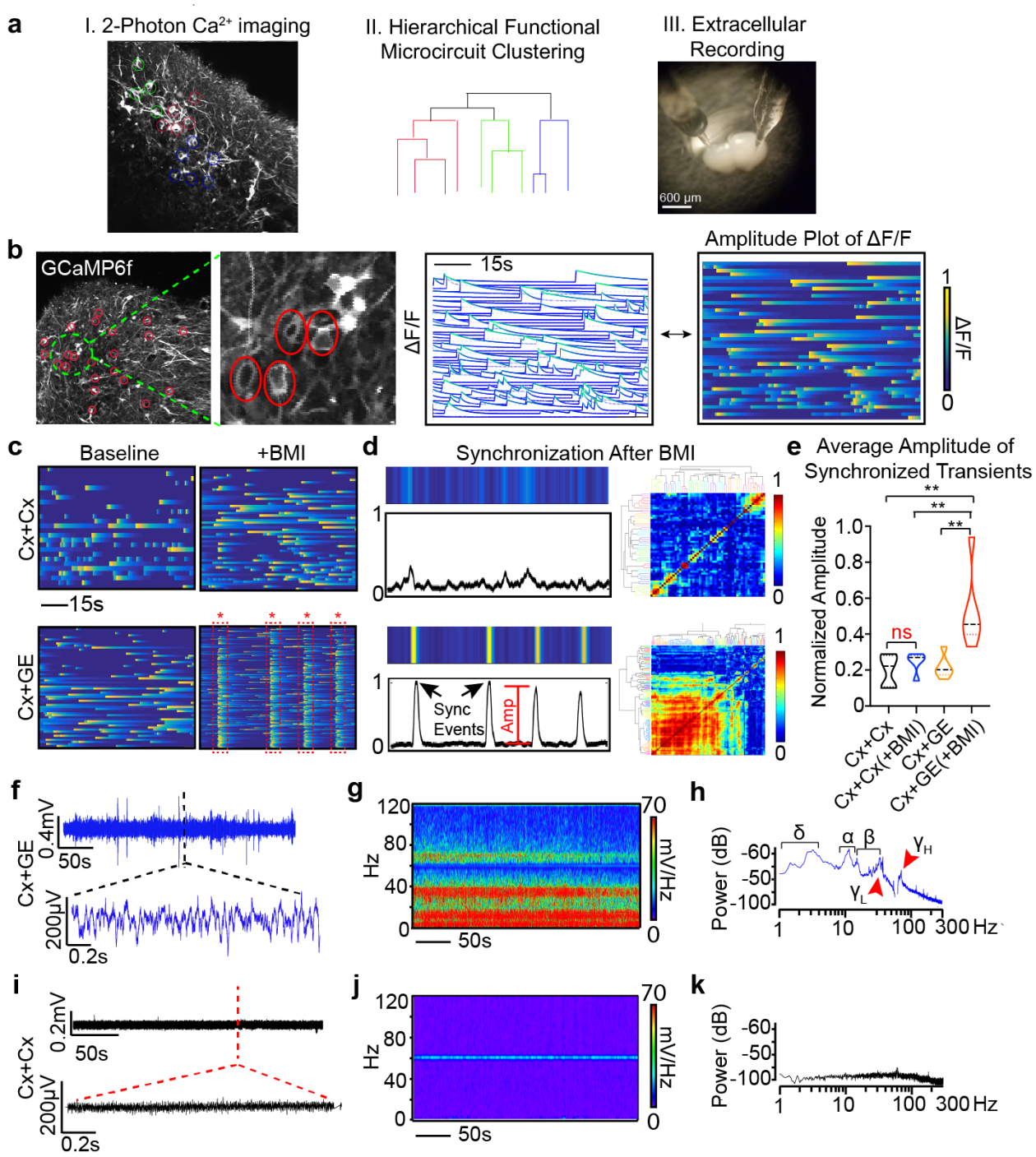

Fig. 2 | Cx+GE fusion organoids demonstrate complex neural network activities. (**a**) Schematic illustrating the identification of active neurons by virtue of their Ca^{2+} transients (I), representation of their network organization (II), and methods used to collect extracellular recordings (III). (**b**) Example of live 2-photon microscopy imaging of an H9 hESC derived

fusion organoid demonstrating acquisition of regions of interest (red circles) and the resulting activity profile shown as normalized change in fluorescence (ΔF/F), where each line is an individual neuron (middle plot) and representation of the same data as a colorized amplitude plot (right). (**c**) Addition of 100 μM bicuculline methiodide (BMI) has a minimal effect on Cx+Cx fusions (top) yet elicits spontaneous synchronization of neural activities in Cx+GE organoids (bottom). (**d**) These synchronizations can be transformed into a normalized amplitude versus time plot for quantitative analyses (left) and further visualized as a clustergram following hierarchical clustering of calcium spiking data (right). (**e**) Pooled data of the amplitude measurements. Plots display the full distribution of individual data points with dotted lines indicating the median and quartile values. $n = 3$ for Cx+Cx and Cx+GE. ANOVA $P = 0.0011$, $F = 8.301$, followed by Tukey's multiple comparison; $^{**}P = 0.0028$ for Cx+Cx vs Cx+GE BMI; $^{**}P = 0.0100$ for Cx+Cx BMI vs Cx+GE BMI; $^{**}P = 0.0031$ for Cx+GE vs Cx+GE BMI. (**f-h**) Local field potentials measured from a representative Cx+GE fusion reveal robust oscillatory activities at multiple frequencies during a 5-minute period, reflected in both raw traces (f) and spectrogram (g). Spectral density analysis (h) demonstrates the presence of multiple distinct oscillatory peaks ranging from ~1-100 Hz. (**i-k)** Cx+Cx fusion organoids by contrast lack measurable oscillatory activities. Representative traces in **(**f-h**)** are taken from 3 independent experiments and in **(**i-k**)** from 4 independent experiments.

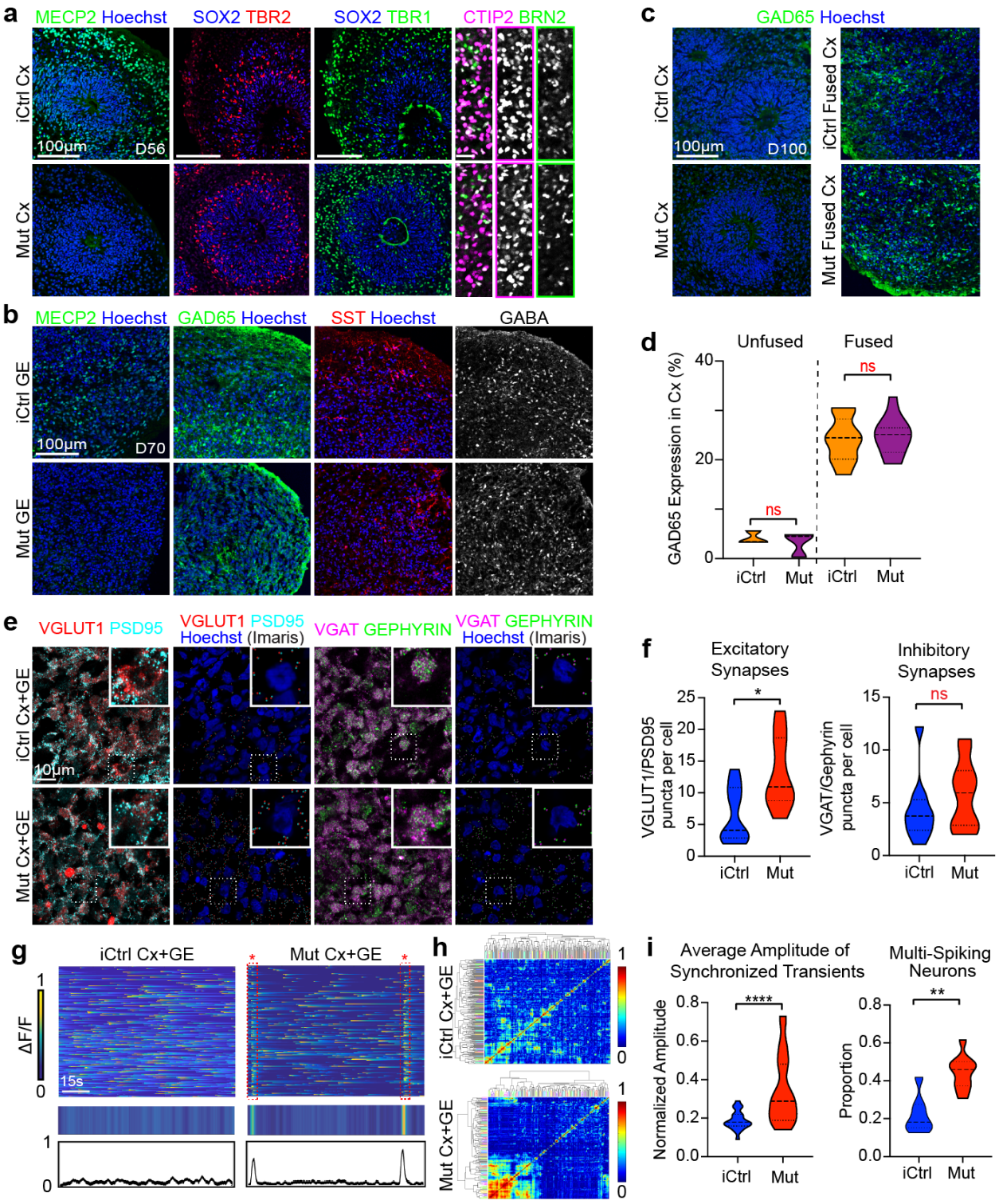

Fig. 3 | Rett syndrome fusion organoids have a higher density of excitatory synapses and exhibit hypersynchronous neural network activity. (**a** and **b**), Generation and

immunohistochemical analyses of isogenic Cx and GE organoids from Rett syndrome patient hiPSC that either contain (iCtrl) or lack (Mut) MECP2 expression. iCtrl and Mut Cx organoids exhibit comparable formation of neural progenitors (SOX2, TBR2), both deep and superficial layer neurons (CTIP2, BRN2), and inhibitory interneurons (GAD65, SST, and GABA). (**c** and **d**) D100 unfused iCtrl and Mut Cx organoids show minimal expression of GAD65, whereas ~20-25% of the cells in the Cx end of age matched Cx+GE organoids express GAD65, $n = 3$ organoids, 2631 cells, ns, not significant. (**e**) Immunohistochemical analysis of excitatory (VGLUT1/PSD) and inhibitory (VGAT/GEPHYRIN) pre-/post-synaptic puncta reveals an increase in excitatory synapses in Mut Cx+GE fusion organoids. Right images display Imaris software renderings of the colocalized pre- and post-synaptic markers used for quantification. (**f**) Plots of the number of synapses per cell. Data were pooled from multiple organoids. VGLUT1/PSD95, $n = 3$ organoids for both iCtrl Mut samples, 1180 cells; VGAT/GEPHYRIN, $n = 4$ organoids for iCtrl and Mut samples, 1654 cells, $^{*}P = 0.0244$. (**g**) Mut Cx+GE fusions exhibit spontaneous synchronized Ca^{2+} transients that are not seen in iCtrl Cx+GE, reflected in the raw ΔF/F colorized amplitude plot (top), synchronization amplitude plot (bottom), and clustergram (**h**). (**I**) Pooled data quantifications, $n = 6$ iCtrl and $n = 7$ Mut fusion organoids, $^{****}P < 0.0001$ for the average amplitude of synchronized transients; $^{**}P = 0.0012$ for multi-spiking neurons. Plots in (d, f**,** i**)** display the full distribution of individual data points with dotted lines to indicate the median and quartile values.

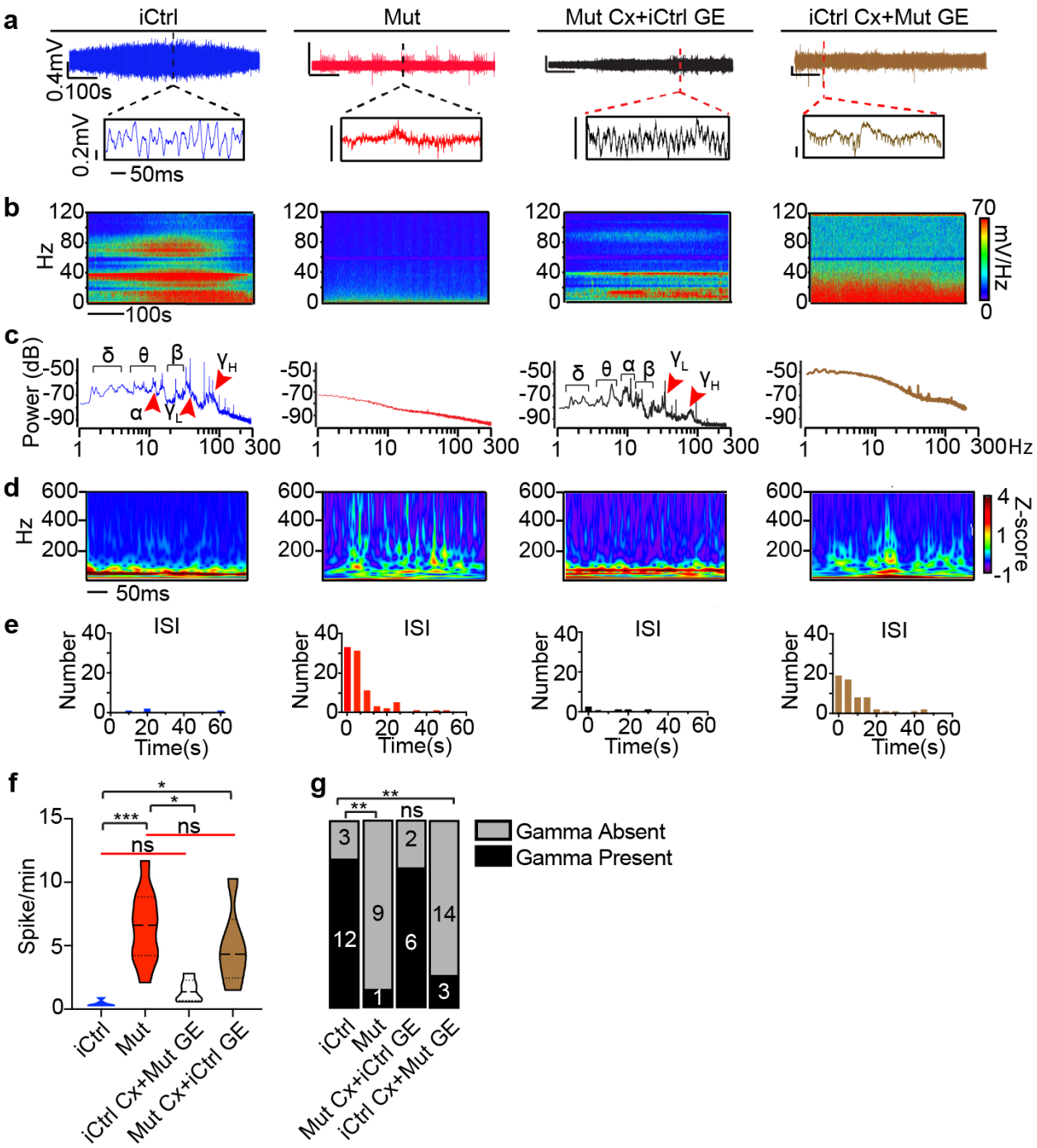

Fig. 4 | Rett syndrome fusion organoids display GE-dependent epileptiform changes. (**a**) Raw trace of a representative 10-minute LFP recording (top) and time expanded window (bottom) from unmixed Mut or iCtrl Cx+GE fusion organoids and Mut/iCtrl mixed Cx+GE fusions. (**b** and **c**) Spectrograms and periodograms derived from the entire recordings shown in

(a). (**d**) Morlet plot showing high frequency activity associated with the time expanded segments shown in (a)**.** (**e**) Frequency histogram of interspike intervals derived from the raw trace in (a). (**i**) Spike frequency across multiple independent experiments Kruskal-Wallis test, overall P=0.0002, Dunn's multiple comparisons ***P = 0.002, *P < 0.05, n = 10 for Mut, n = 6 for all others. Plot displays the full distribution of individual data points with dotted lines to indicate the median and quartile values. (**g**) Tabulation of the number of independent experiments that demonstrated sustained gamma oscillations (~40-80 Hz) within the Cx+GE organoids. Chi square, df = 1 with correction for multiple (3) comparisons, iCtrl vs. Mut **P = 0.003, iCtrl vs. iCtrl Cx+Mut GE **P = 0.0012.

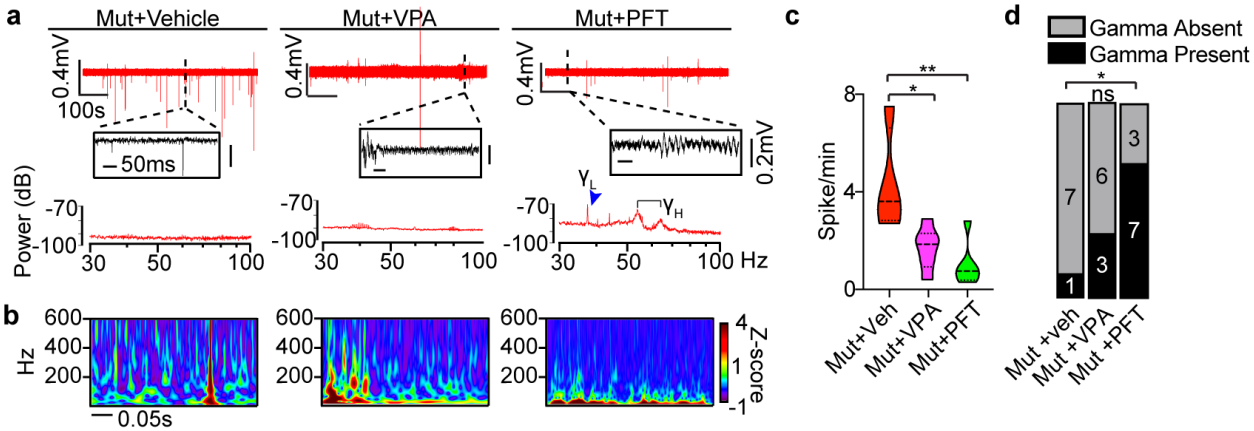

Fig. 5 | Partial restoration of gamma oscillations and suppression of HFOs in Rett syndrome fusion organoids by administration of Pifithrin-α. (**a**) Raw trace (top), time expanded window (middle), and periodogram (bottom) from representative Mut Cx+GE fusion organoids treated for 48 hr with vehicle (DMSO, Veh), 2 mM sodium valproate (VPA), or 10 μM Pifithrin-α (PFT). (**b**) Morlet plot derived from the time expanded segment in (a). (**c**) Spike Frequency following drug addition; Kruskal-Wallis test, overall P=0.0020, Dunn's multiple comparisons **P = 0.0042, *P < 0.05, n=5 for Mut+Veh, n = 6 Mut+VPA, n = 7 Mut+PFT. Plot displays the full distribution of individual data points with dotted lines to indicate the median and quartile values. (**d**) Tabulation of the number of independent experiments that demonstrated sustained gamma oscillations (~40-80 Hz) within the Mut Cx+GE organoids. Chi square, df = 1 with correction for multiple (3) comparisons. Mut+Veh vs. Mut+PFT, *P = 0.04; Mut+Veh vs. Mut+VPA, not significant (ns, P > 0.05).